Thermochimica Acta 635 (2016) 41–58

Contents lists available at ScienceDirect

Thermochimica Acta

journal homepage: www.elsevier.com/locate/tca

The effect of heat treatment on the mechanical and structural properties of one-part geopolymer-zeolite composites

P. Sturm[a,*], G.J.G. Gluth[a], S. Simon[b], H.J.H. Brouwers[c], H.-C. Kühne[a]

[a] Division 7.4 Technology of Construction Materials, Bundesanstalt für Materialforschung und -prüfung (BAM), Berlin, Germany
[b] Division 7.1 Building Materials, Bundesanstalt für Materialforschung und -prüfung (BAM), Berlin, Germany
[c] Department of the Built Environment, Eindhoven University of Technology, Eindhoven, The Netherlands

ARTICLE INFO

Article history:
Received 26 October 2015
Received in revised form 12 February 2016
Accepted 21 April 2016
Available online 23 April 2016

Keywords:
Geopolymers
Zeolites
Alkali-activation
High-temperature treatment
Thermal behavior
Nepheline

ABSTRACT

This contribution presents the results of structural and compressive strength investigations on cured and high-temperature treated silica-based one-part geopolymer-zeolite composites. The specimens were synthesized from two different silica sources, sodium aluminate and water. The phase content as well as the compressive strength of the cured composites varied depending on the starting mix-design and the silica feedstock. Besides geopolymeric gel, A-type zeolites and hydrosodalites were the major reaction products. One of the silica feedstocks yielded significantly higher compressive strength (19 MPa), while the other one appears to cause less variation in phase content. Strength testing indicated an improvement on heating up to 200–400 °C (28 MPa) followed by a moderate decrease up to 700 °C. Above 700 °C the systems underwent new phase formation and shrinkage (volume decrease) deformations. After exposure at 1000 °C the different mixes consisted of a mix of several stuffed silica phases, almost pure hexagonal nepheline or amorphous phase. Depending on the mix-design, the onset temperature of the high temperature phase transformations varied.

1. Introduction

Geopolymers are aluminosiliceous compounds whose network structure closely resembles those of zeolites [1–4]. The geopolymeric gel is amorphous to X-rays, but in many cases the material contains crystalline zeolites. The geopolymeric gel can be regarded as metastable amorphous zeolites that were unable to crystallize due to deficiency in water in the reaction system [5–7]. Geopolymers can form the basis of concretes with much lower related CO_2 emissions than concretes based on conventional Portland cement [8]. In addition to this environmental benefit, geopolymers, when properly designed, can possess beneficial engineering properties, such as high chemical durability [9,10] and good resistance against high temperatures [11–15]. The latter makes them particularly interesting for fire-resistant coatings and refractories [16–19], and also for production of ceramics [20–22]. However, some geopolymer systems exhibit significant shrinkage during dehydration due to the release of "structural" water (*e.g.* Ref. [23]), which is a problem in construction and high-temperature applications.

Recent approaches have focused on so called "one-part" geopolymer mixes [24–29]. The synthesis route for these formulations is similar to the procedure for the hydration of conventional Portland cement-based binders. For example, one-part geopolymers can be produced from mixed silica and alumina sources incorporating the alkalis in water-soluble form, thus, just water has to be added. There is no necessity to handle highly alkaline solutions, because the solution forms directly in the reaction system by dissolution of the solid starting material(s). This can provide a higher social and economic acceptance compared to conventional geopolymers [24,30].

Compared to conventional "two-part" geopolymers (*i.e.* geopolymers from a solid aluminosilicate feedstock and a highly alkaline solution), much less is known about the thermal properties of one-part geopolymers, and experience with the former cannot be simply transferred to the new systems. Therefore, the present contribution investigates one-part geopolymers-zeolite composites in terms of compressive strength performance and phase development during elevated to high temperature treatment.

* Corresponding author.
E-mail address: patrick.sturm@bam.de (P. Sturm).

http://dx.doi.org/10.1016/j.tca.2016.04.015
0040-6031/

Table 1
Chemical composition of the feedstocks.

Component	MS (wt.%)	CR (wt.%)	$NaAlO_2$ (wt.%)
SiO_2	95.16	84.23	0.61
Al_2O_3	0.17	4.18	60.85
Fe_2O_3	0.04	0.43	0.06
TiO_2	<0.01	0.06	0.00
CaO	1.71	2.97	0.26
MgO	0.28	0.17	0.02
Na_2O	0.19	0.22	36.07
K_2O	0.65	0.03	0.03
SO_3	0.25	0.16	0.16
Cl^-	n.d.	1.36	n.d.
LOI	1.12	5.08	1.73

n.d.: not determined; LOI: loss on ignition.

2. Experimental

2.1. Starting materials

One-part mixes were synthesized from two different silicas and sodium aluminate. A commercial microsilica (referred to as MS) and an industrial residue from the chlorosilane production (referred to as CR) were used as silica sources. All feedstocks were characterized by chemical analysis (inductively coupled plasma optical emission spectrometry (ICP-OES) after microwave digestion) and X-ray diffraction (XRD). MS contained 95.2 wt.% SiO_2, CR contained 84.2 wt.% SiO_2. The medians of the particle size distributions were d_{50} = 0.19 μm for silica MS and d_{50} = 6.83 μm for silica CR. SEM investigations indicated an average size of the primary particles of about 100–200 nm (MS) and 50–200 nm (CR) [26], respectively. XRD showed only an "amorphous hump" for the MS feedstock and minor amounts of silicon carbide (PDF # 01-089-3167) (Fig. 1). CR diffractograms indicate, besides amorphous phase, minor crystalline impurities calcite (PDF # 01-086-0174) and quartz (PDF # 00-046-1045). In contrast to calcite, the quartz impurity was not observed in all samples, and the included quartz was found at amounts only slightly above the detection limit. Results of the chemical analysis are presented in Table 1. The loss on ignition (LOI) for CR is higher than for MS; this is due to the incorporated calcite.

The sodium aluminate had an almost stoichiometric Na/Al ratio of 0.98 mol/mol. Besides dry sodium aluminate (PDF # 00-033-1200), XRD (Fig. 1) also indicated very small amounts of hydrated sodium aluminate (PDF # 01-083-0315) and, because of the carbonation tendency of the material, some natrite (PDF # 01-072-0628). The loss on ignition (LOI) of 1.73 wt.% (including ~0.2 wt.% CO_2) is in line with the identified low amounts of hydrated phase in the diffractogram.

2.2. Sample preparation

For the synthesis of the one-part mixes, the solid feedstocks were mixed to yield specific silica/alumina ratios (SiO_2/Al_2O_3 mol/mol). After the addition of water at a nominal water/binder-ratio (w/b) by mass of 0.50, pastes were mixed using a contact free planetary centrifugal mixer (2000 rpm; 2 min). Pastes were then cast into 20 mm × 20 mm × 20 mm cube moulds and compacted by tapping the moulds on the lab bench. Subsequently the samples were cured at 80 °C and 80% r. H. in an oven with climate control for three days. Table 2 presents sample nomenclature and mix designs for the binder pastes.

Some pastes were produced in duplicate to measure the pH value in the paste within the first 30 min after the addition of water. In addition, pH measurements were done on various sodium aluminate solutions. All Measurements were conducted using a METTLER DELTA 350 device with Metrom pH-electrode. Calibration of the electrode was done with standard buffer solutions of pH 7 and pH 10.

Cube specimens were used for compressive strength tests in the initial (as cured) state and for the residual strength tests after further temperature treatment. After one day of curing samples were removed from the moulds and cured for further two days at 80 °C and 80% r. H. After the complete curing period of 3 days they were stored 1–7 days at 23 °C and 50% r. H in a climate chamber until required for testing or heating. After heating and strength testing fracture pieces for the structural investigations were stored in a desiccator over dried silica gel at ambient temperature. Grinding was done manually with mortar and pestle (agate) to provide a preparation as gently as possible, in particular for samples during dehydration.

2.3. Thermogravimetric analyses and thermal treatment

Thermogravimetric (TG) investigations were conducted with a Netzsch device (STA 449C Jupiter) in N_2 atmosphere at a heating rate of 5 K min^{-1}, treating ~20 mg sample mass. The thermal treatment of the cube specimens was realized in a muffle furnace (Carbolite CWF 12/5; T_{max} = 1200 °C). The samples were transferred to the furnace at ambient temperature and heated to the target temperature using a ramp program (1 K min^{-1}) to avoid excessive temperature gradients in the specimens. The desired temperature was held for three hours. Afterwards the samples were allowed to cool down naturally to ambient temperatures in the furnace followed by an immediate testing of the compressive strength.

2.4. Structural investigations

XRD measurements were done with a Rigaku Ultima IV device using Cu Kα radiation (λ = 1.5419 Å), Bragg-Brentano geometry, a 10 mm divergence slit, sampling steps of 0.01° 2θ and a sampling speed of 0.2° 2θ min^{-1} (1° 2θ min^{-1} for the sodium aluminate) in the scanning range 3–63° 2θ.

Attenuated total reflection Fourier transform infrared spectroscopy (ATR FT-IR) measurements were conducted using a Bruker Tensor 27 device with a diamond ATR module (measuring range: 4000–400 cm^{-1}; resolution 4 cm^{-1}; scans: 16; detector: RT-DLaTGS).

SEM investigations were performed using a Carl Zeiss EVO MA10 device with a secondary electron (SE) detector and an accelerating voltage of 7–10 kV. Samples were sputtered with gold before measurements.

2.5. Compressive strength testing

The compressive strength performance testing was conducted with a ToniPRAX device on the 20 mm × 20 mm × 20 mm cubes at a loading rate of 240 N/s (equivalent to 0.6 MPa/s for the investigated samples). Strength testing was also done on cube samples heated to temperatures between 100 °C and 750 °C (MS mixes) and 800 °C (CR mixes). For each cured and thermal treated one-part mix three experiments were conducted and the means of the results are presented.

2.6. Dilatometry

The dilatometry measurements were conducted with a vertical dilatometry device (Bähr TMA 801) between ambient temperature and 900 °C. Samples were prepared with a high precision diamond saw blade to form square tablets of 5 mm height and ~5 mm side lengths. Samples were heated at a rate of 5 K min^{-1} in an air atmo-

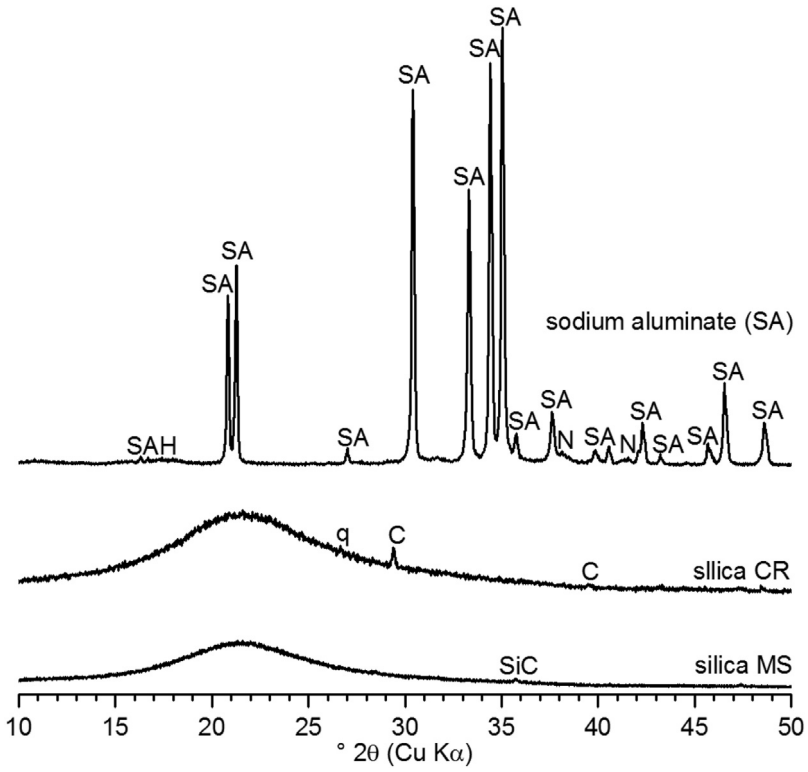

Fig. 1. Diffraction patterns of the feedstocks (SA = sodium aluminate; SAH = sodium aluminate hydrate; N = natrite; q = quartz; C = calcite, SiC = silicon carbide). The sodium aluminate sample was measured with a speed of 1° 2θ per minute because of its hygroscopic character.

Table 2
Mix-designs of the one-part composites.

Sample series	m(Na_2O) (wt.%)	m(Al_2O_3) (wt.%)	m(SiO_2) (wt.%)	m(H_2O) (wt.%)	Na_2O/Al_2O_3 (mol/mol)	SiO_2/Al_2O_3 (mol/mol)	H_2O/Al_2O_3 [mol/mol]
CR_2	12.70	22.63	26.88	34.15	0.92	2.02	8.54
CR_3.5	9.13	16.99	35.19	34.09	0.88	3.51	11.35
CR_6	5.98	12.01	42.55	34.03	0.82	6.01	16.04
MS_2	13.75	23.16	27.53	34.24	0.98	2.02	8.37
MS_3.5	10.42	17.52	36.31	34.20	0.98	3.52	11.05
MS_6	7.43	12.46	44.19	34.17	0.98	6.02	15.51

sphere. The loading force was 0.05 N. Relative changes of samples height were recorded during heating.

3. Results and discussion

3.1. pH measurements

Besides the kind of silica feedstock, the behavior of the sodium aluminate plays an important role for the evolution of the phase content of the one-part mixes. It is known that in the Na_2O-Al_2O_3-H_2O system at temperatures up to 150 °C the equilibrium concentration of Na is always higher than that of Al (also when Cl^- or CO_3^{2-} impurities are present) [31], *i.e.* in $NaAlO_2$ solutions the precipitation of $Al(OH)_3$ is expected. This is confirmed by our own auxiliary experiments, in which it was found that a sodium aluminate suspension (25 g sodium aluminate in 50 g water) rapidly precipitates a white gel. XRD analyses (results not shown) revealed that after several days aging at 80 °C the gel had crystallized to gibbsite (PDF # 00-033-0018); no sodium-containing phase was found in the precipitation product. The pH of the sodium aluminate suspension was determined 10 min after the addition of water to be 14.4. A sodium aluminate suspension with 28.48 g sodium aluminate suspended in 25.00 g water, *i.e.* simulating the conditions in MS_2 and CR_2 (*cf.* Table 2), had pH = 14.7 after 8 min.

pH measurements were also conducted on the fresh pastes: The MS_2 paste had pH = 14.5 10 min after adding water, and pH = 14.7 after 30 min. CR_2 pastes had pH = 14.7 after 10 min. On the contrary, the fresh high-silica (SiO_2/Al_2O_3 = 6) pastes had pH values of only 14.2 (MS_6) and pH = 13.4 (CR_6) after 10 min. These results will be further discussed below in connection with phase assemblage of the cured materials.

3.2. Structural properties of the cured specimens

XRD investigations (Fig. 2) showed that in addition to an amorphous gel phase significant amounts of crystalline phases formed in the reaction products. Thus, the products obtained after curing are more properly termed geopolymer-zeolite composites, rather than geopolymers. Depending on the silica feedstock and the mix-design of the starting mix, differences in the phase content of the hardened samples were observed, as is detailed in the following paragraphs. In the discussion that follows it is assumed that a higher relative intensity of a particular phase in a diffractogram corresponds to a higher fraction of that phase in the investigated material, compared to a material with lower intensities of that phase. Though no quantitative analysis (*e.g.* Rietveld analysis) of the diffractograms has been undertaken, it is assumed that this approach allows at least a semi-quantitative interpretation of the results, particularly

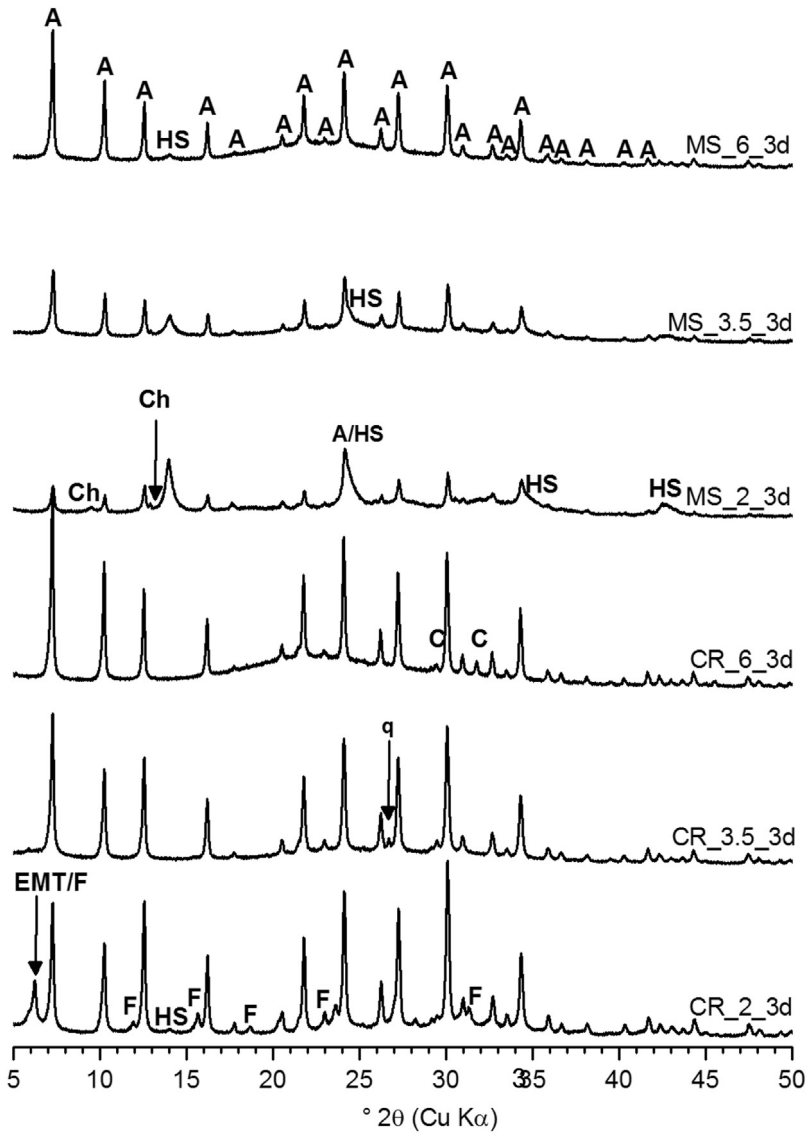

Fig. 2. Diffraction patterns of the geopolymer-zeolite composites systems after 3 days of curing (A = zeolite A; HS = hydrosodalite, Ch = chabazite; F = faujasite; EMT = zeolite EMT; C = calcite; q = quartz).

since all the observed major crystalline phases have a cubic crystal structure, and thus preferred orientation effects are absent.

The hump, representing amorphous phase, is located at ca. 15°–35° 2θ in the diffractograms (Fig. 2). Compared to the silica feedstock (Fig. 1) the hump is broadened and/or shifted to higher 2θ. For high silica mixes (SiO_2/Al_2O_3 = 6 mol/mol) the maximum of the hump was located at ~22° 2θ. This was the same value as for the silica feedstocks (Fig. 1). However, the hump is broadened and in addition to the first maximum, a second maximum at ~30° 2θ could be detected. For the low silica mixes (SiO_2/Al_2O_3 = 2 mol/mol) the hump was shifted to higher 2θ and had its maximum at ~30° 2θ. The samples with intermediate silica/alumina ratio (SiO_2/Al_2O_3 = 3.5 mol/mol) exhibited a behavior somewhere in between, *i.e.* the hump was shifted slightly with a maximum in the range 22–30° 2θ. In a previous investigation [28] it was shown that the low-silica sample (MS_2) contains no residual silica feedstock after curing, thus the hump with the maximum at ~30° 2θ can be assigned to the geopolymeric gel, in accordance with literature data [32]. From these observations it can be concluded that the hump in the mixes with higher SiO_2/Al_2O_3 ratios is caused by contributions from geopolymeric gel and remaining silica material.

For microsilica (MS)-based one-part mixes (MS_2, MS_3.5, MS_6) dominant crystalline phases were hydrated zeolite A (PDF # 00-039-0222) and non-basic hydrosodalite of intermediate water content, $Na_6(AlSiO_4)_6{\cdot}4H_2O$ (PDF # 00-042-0216). This hydrosodalite has been found previously in geopolymer systems with low silica starting contents [25,28,33]. Depending on the chemical composition of the starting system the two primary crystalline reaction products varied in their quantities. With decreasing silica content the relative amount of hydrosodalite *versus* zeolite A increased, as has been reported previously [28]. Both phases are presented in all MS-based specimens and, except in the low-silica samples MS_2 (SiO_2/Al_2O_3 = 2 mol/mol), zeolite A is always the main phase of the reaction products.

Medium-silica (MS_3.5), and particularly the low-silica samples (MS_2) may include higher hydrated forms of hydrosodalite, *e.g.* $Na_6(AlSiO_4)_6{\cdot}8H_2O$ (PDF # 00-040-0102), and/or basic hydrosodalite ($Na_8(AlSiO_4)_6OH_2{\cdot}xH_2O$) (PDF # 00-040-0101; PDF # 00-041-0009), which have quite similar peak positions, noticeable as asymmetric peak shapes of the main peaks (*cf.* Section 3.3). Fur-

thermore, because of the fairly broad shape and low maximum intensities of the diffraction pattern of MS_2, especially of the main peaks of hydrosodalite, it can be assumed that basically heterogeneous sodalite structures with rather small crystallite sizes [33–35] appear in the reaction system. In addition, the MS_2 mix contained small amounts of chabazite, $NaAlSi_2O_6{\cdot}3H_2O$ (PDF # 00-019-1178), a zeolite with increased silicon content compared to zeolite A and hydrosodalite.

For CR-based mixes (CR_2, CR_3.5, CR_6) zeolite A was always the dominant crystalline phase. Besides zeolite A, no further crystalline aluminosilicate phase could be observed by XRD in intermediate and high-silica specimens (CR_3.5, CR_6). Only the low-silica specimens (CR_2) contained small amounts of hydrosodalite (Fig. 2). In addition, faujasite (PDF # 00-038-0239) occurred in the latter samples; a shoulder at the main peak indicates also the presence of zeolite EMT (PDF # 00-046-0566). These two zeolites tend to form (disordered) intergrowths [36,37]. Besides crystalline and amorphous reaction products also remaining impurities (calcite, quartz) from the silica feedstock (CR) were observed (Fig. 2).

The differences in the phase content of the cured composites can be partly explained by the differences in pH of the fresh pastes (Section 3.1): The higher pH in the MS_2 mix is assumed to be the reason for direct formation of hydrosodalite or early transformation of zeolite A into hydrosodalite structures (*cf.* Ref. [38]). However, it is not clear at present why hydrosodalite formation is much more pronounced in the MS-based composites, compared to the CR-based ones. The higher pH in the low-silica samples (MS_2 and CR_2) will also cause faster dissolution of the silica in the hardening pastes. This is possibly the reason for the formation of chabazite, or faujasite and zeolite EMT in the MS_2 and CR_2 samples, respectively. These zeolites have an anionic framework with silicon excess over aluminium (Si:Al > 1), which implies a faster dissolution of the silica, and are only present in the low-silica mixes.

The relative intensities of the three peaks of zeolite A at lowest diffraction angles (7.17°, 10.16° and 12.47° 2θ) varied in the samples (Fig. 2). For reference zeolite A (*e.g.* PDF # 00-039-0222) their intensities are decreasing from the first (7.17° 2θ) over the second (10.16° 2θ) to the third (12.47° 2θ). However, depending on the mix-design of the composites the intensity of the third of these peaks was increased, in particular for the low-silica mixes. This is most likely related to small variations of stoichiometry (Si:Al ratio) and water content of the A-type zeolites framework: In the diffractograms of conventionally synthesized zeolite A samples, presented by Radulović et al. [39], comparable changes in peak intensities are observed on going from $1.05Na_2O{\cdot}1.06Al_2O_3{\cdot}2.00SiO_2$ to $1.05Na_2O{\cdot}1.00Al_2O_3{\cdot}2.05SiO_2$, though the cell parameters of the zeolites did not differ significantly. In addition, calculated XRD patterns of hydrated and dehydrated zeolite A [37] reveal a more pronounced decrease of the peak height of the third peak on dehydration, compared to the height of the other two peaks at lower 2θ. Comparable tendencies were observed during heating (dehydration) of the considered composite samples (Section 3.4).

3.3. Thermogravimetric analyses

Since zeolite A is the dominating crystalline phase in most of the considered samples, TG analysis was also performed on a reference zeolite A sample (Henkel AG & Co. KGaA, Düsseldorf, Germany). The average crystallite size of the reference zeolite A was ~1 μm (as observed with SEM; results not shown), and it contained only a marginal amount of hydrosodalite as impurity (checked by XRD as well as ^{29}Si and ^{27}Al MAS NMR; results not shown). Its dehydration behavior was compared to those of the cured composites, and selected temperature points were determined for additional structural and mechanical investigations (Fig. 3). Mass loss for both, the quasi-pure zeolite A and the geopolymer-zeolite composites, ran quite similar with different absolute amounts. At 400 °C the major part of the dehydration was completed. All samples contained small amounts surface water noticeable as mass loss below 100 °C (Table 3, Fig. 3).

Zeolite A exhibited a stepwise dehydration behavior with a steep loss up to ~200 °C and a second step with lower slope between 200 °C and 400 °C. The geopolymer-zeolite composites exhibited a rather continuous behavior with the TG curve flattening due to a slower water release with increasing temperature. However, the MS_2 specimen exhibited a multiple-step mass loss at higher temperatures, most likely due to several incorporated hydrosodalite structures (see below).

For the composites the most dominant mass loss of 6.2–8.4 wt.% occurred between 100 °C and 200 °C (for comparison: zeolite A: 12.3 wt.%). A further significant mass loss of 2.5–5.3 wt.% (zeolite A: 3.7 wt.%) followed between 200 °C and 400 °C. This dehydration range correlates quite well with reported TG data for zeolite A and hydrosodalites [34,40–42].

In general, in each class of geopolymer-zeolite composites (*i.e.* CR-based or MS-based), the final mass loss at 1200 °C decreased with increasing SiO_2/Al_2O_3 ratio. This is related to the fact that only in the low-silica samples ($SiO_2/Al_2O_3 = 2$) the silica feedstocks react virtually completely, while in the mixes with higher SiO_2/Al_2O_3 ratios the silica reacts only partly, the fraction of remaining silica being larger at higher SiO_2/Al_2O_3 ratios [28]. This means that at higher SiO_2/Al_2O_3 ratios the fraction of porous reaction products (zeolites and geopolymeric gel) in the cured specimens is generally lower, and correspondingly the total water content is lower.

Deviating from this general trend, the MS_2 sample exhibited a peculiar behavior in that its mass loss up to ca. 900 °C was lower than the mass loss of MS_3.5 (and virtually the same at 1200 °C) and that distinct steps can be distinguished in the TG curve in the range 400–900 °C. Felsche and Luger [40] reported a double-step dehydration (two overlapping DTG peaks) of fully hydrated non-basic hydrosodalite ($Na_6(AlSiO_4)_6{\cdot}8H_2O$) in the range of ca. 60–340 °C and a multiple-step dehydration and dehydroxylation of *presumed* basic hydrosodalite ("$Na_8(AlSiO_4)_6OH_2{\cdot}4H_2O$") in the range ca. 80–810 °C. In a subsequent study [42] the result for $Na_6(AlSiO_4)_6{\cdot}8H_2O$ was confirmed (double-step dehydration in the range 100–350 °C), but it was found that basic hydrosodalite, $Na_8(AlSiO_4)_6OH_2{\cdot}2H_2O$, exhibits a double-step dehydration (two overlapping DTG peaks) in the range ca. 530–700 °C. The study furthermore proved that basic hydrosodalites with more than 2 mol hydration water ($Na_8(AlSiO_4)_6OH_2{\cdot}2H_2O$) are actually a mix of basic and non-basic hydrosodalites. The TG curve of MS_2 is comparable to the curve presented in Ref. [40] for "$Na_8(AlSiO_4)_6OH_2{\cdot}4H_2O$", which was found later to be a mix of basic and non-basic hydrosodalites [42]. Taking also into account the XRD peak shapes (see Section 3.2), it is tentatively concluded that this sample contained, besides non-basic hydrosodalite of intermediate water content, also smaller amounts of basic hydrosodalite and possibly non-basic hydrosodalites of different water content.

All CR-based samples exhibited a distinct step around 850–1000 °C. This step is related to the impurities in the CR-based systems: these contained calcite from the silica feedstock (Figs. 1 and 2), which decomposes in that temperature range.

3.4. Structural changes during thermal treatment

XRD experiments were conducted to identify structure changes and phase transformations during the dehydration (main part up to 400 °C), up to the "breakdown" of the structure between 650 °C and 750 °C and the new phase formation up to 1000 °C. Since the samples were allowed to cool down to ambient in the furnace before testing, rehydration of zeolites as well as retrograde phase

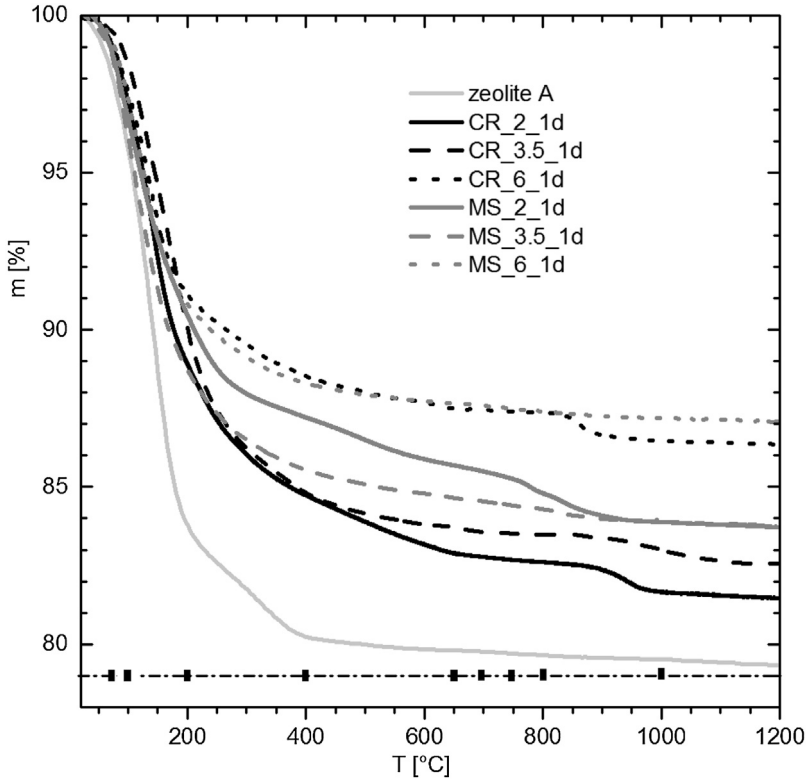

Fig. 3. TG curves of the composites after 3 days of curing and zeolite A. Squares represent temperatures chosen for XRD investigations and residual compressive strength testing.

Table 3
Residual masses of the samples during TG analysis.

Sample	$m_{r\,(100\,°C)}$ (wt.%)	$m_{r\,(200\,°C)}$ (wt.%)	$m_{r\,(400\,°C)}$ (wt.%)	$m_{r\,(650\,°C)}$ (wt.%)	$m_{r\,(700\,°C)}$ (wt.%)	$m_{r\,(750\,°C)}$ (wt.%)	$m_{r\,(1000\,°C)}$ (wt.%)
CR_2	97.2	88.9	84.8	82.9	82.8	82.7	81.7
CR_3.5	98.5	90.1	84.8	83.7	83.5	83.5	83.0
CR_6	97.6	91.1	88.5	87.5	87.5	87.4	86.5
MS_2	96.7	90.5	87.2	85.7	85.5	85.3	83.9
MS_3.5	96.1	88.7	85.5	84.7	84.5	84.4	83.9
MS_6	97.3	90.8	88.3	87.7	87.6	87.5	87.2
zeolite A	96.3	84.0	80.3	79.8	79.8	79.7	79.5

formation cannot be fully excluded. Up to specific temperatures, at least 650 °C, basically no major phase transformations could be observed. Above this temperature completely new structures occur with significant differences between the different mix-designs (Figs. 4–11). Equally composed mixes (*i.e.* mixes produced from different silica feedstocks but with identical SiO_2/Al_2O_3 ratio) showed comparable behavior.

Fig. 4 presents the XRD patterns of the mix CR_2 after heating to specific temperatures up to 1000 °C. Up to 400 °C, except the disappearance of faujasite and a decrease of the third zeolite A peak at 12.47° 2θ, no significant changes could be observed by XRD. Other small changes of the absolute intensities in the range of moderate temperature treatment are not regarded significant due to the influence of the preparation with mortar and pestle.

At 650 °C first significant structure transformations occurred. Only zeolite A remained, all peak intensities decreased significantly and the FWHMs (full widths at half maximum) of the peaks increased, probably attributable to commencing of structural breakdown. A new peak occurred (21.4° 2θ), indicating the initial formation of a new phase.

At 700 °C this "metaphase" and nepheline, $NaAlSiO_4$ (PDF # 00-035-0424), were the new main phases. Most peaks of the pattern can be matched with the nepheline reference, but the reflection of maximum intensity located at 21.4° 2θ was exaggerated. At 700 °C intensities were increased and FWHMs decreased compared to 650 °C as a result of further crystallization. Several studies [21,39,43] found low carnegieite, $NaAlSiO_4$, as a metaphase during the transformation of geopolymers and A-type zeolites to stuffed tridymite structures (nepheline), and reported the position of the diagnostic main peak to be in the same 2θ-range as the observed exaggerated peak at 21.4° 2θ. However, with the available carnegieite reference (PDF # 96-101-0954) this peak could not be matched satisfyingly. Since the composition of stuffed silica structures is variable [44,45], a carnegieite-type phase of intermediary composition is possible. In addition to the aforementioned phases, sodalite *sensu stricto*, $Na_8(SiAlO_4)_6Cl_2$, (PDF # 00-037-0476) was observed in the heated CR_2 samples (chloride provided by the silica feedstock CR). Only residues of zeolite A remained in the sample.

At 750 °C again a further phase transition was apparent. Nepheline was clearly the new main phase, and the exaggeration of the main peak at 21.4° 2θ decreased. Sodalite, which is known to coexist with nepheline [46], remained in the system, but no zeolite A. At 800 °C the system was almost equal to that at 750 °C, only the

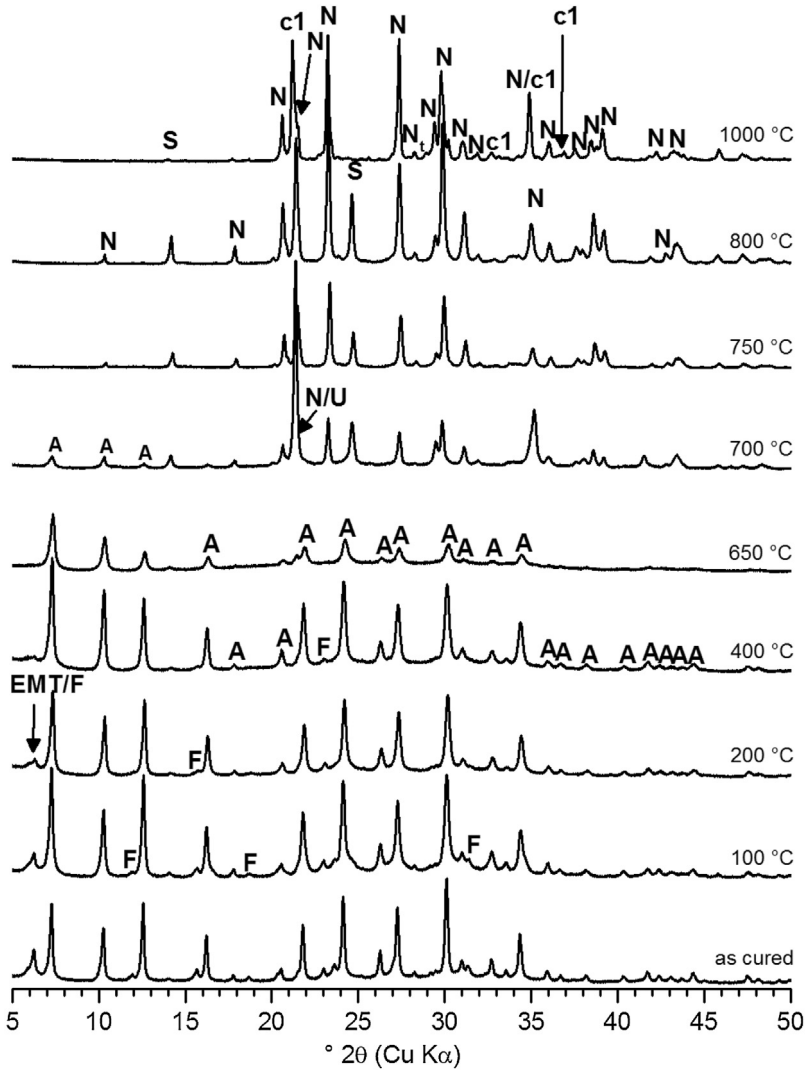

Fig. 4. Diffraction patterns of temperature-treated CR_2 mix. (A = zeolite A; F = faujasite, EMT = zeolite EMT; N = hexagonal nepheline; N_t = monoclinic trinepheline, S = sodalite sensu stricto, c1 = intermediary carnegieite structure; U = unknown metaphase).

crystallinity was increased and exaggeration of the peak at 21.4° 2θ decreased further.

After exposure to the highest investigated temperature of 1000 °C most of the peaks are still related to nepheline, but the position of the main peak slightly shifted to lower value (21.19° 2θ), thus nepheline fitted only the shoulder of that peak. Thompson et al. [44,45] reported several tectosilicates of carnegieite structure synthesized at high temperatures and noted the problem of reaching equilibrium below 1300 °C because of the slow reaction kinetics. However, one of the reported intermediary structures ($Na_{1.45}Al_{1.45}Si_{0.55}O_4$, PDF # 00-049-0002) [44] matches the two diagnostic peaks of CR_2 after 1000 °C at 21.10° 2θ and 34.83° 2θ (Fig. 4) although the second peak is covered by nepheline, too. This is in line with previous studies on the high-temperature behavior of geopolymers [21,43], which reported the formation of dominating hexagonal nepheline and carnegieite above 800 °C. A further diagnostic peak occurred after 1000 °C at 28.2° 2θ and is related to monoclinic trinepheline.

Fig. 5 shows the evolution of sample MS_2. Except the decrease of the third zeolite A peak, up to 650 °C no major changes were observed and generally crystallinity remained poor. The intensity of the main peak of hydrosodalite, located at ~24.7° 2θ, decreased compared to the second diagnostic peak at 13.97° 2θ. Felsche and Luger [41] reported a water-free form of sodalite, $Na_6(SiAlO_4)_6$, (PDF # 00-040-0101), that exhibits the same "reversed" intensities as observed in the diffractograms of MS_2 after dehydration. The small zeolite A peaks underwent no visible changes up to 700 °C. Above 200 °C no chabazite remained.

At 750 °C a significant phase transformation was observed. Nepheline was the new main phase. The main peak was again exaggerated, but less intensive compared to CR_2. Only minor amounts of zeolite A and the supposed water-free sodalite were left. A small reflection appeared at 9.75° 2θ, which could not be assigned to a particular phase. Overall, the pattern at 1000 °C appears quite similar to the one at 750 °C, although few additional small peaks occur that can be matched with the intermediate stuffed cristobalite phase. In contrast to CR_2, small amounts of carnegieite (PDF # 96-101-0954) could be clearly identified at this temperature, as was also found in Refs. [21,43]. Again monoclinic trinepheline was present as additional phase; the unassigned reflection at 9.75° 2θ disappeared.

For sample CR_3.5 (Fig. 6) no significant changes could be observed up to 650 °C except the diminishment of the third zeolite A peak at 12.48° 2θ. At 700 °C the first significant changes occurred. The crystallinity started to decrease, eventually leading to an almost complete structure breakdown at 750 °C, comparable to the behav-

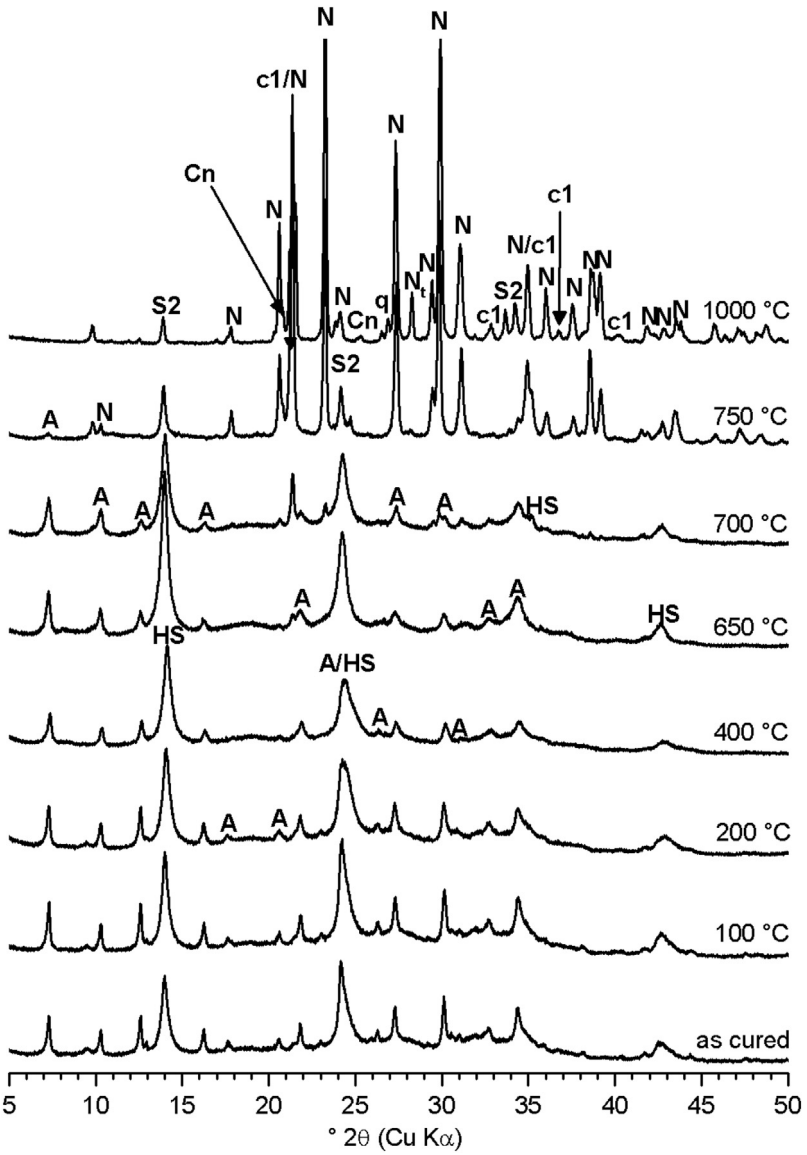

Fig. 5. Diffraction patterns of temperature-treated MS_2 mix. (A = zeolite A, HS = hydrosodalite, N = nepheline; N_t = monoclinic trinepheline; S2 = dehydrated HS; c1 = intermediary carnegieite structure; Cn = carnegieite).

ior of almost stoichiometric zeolite A, but at lower temperature [39]. Only residues of zeolite A remained as well as a very small not identified peak at the position of faujasite's main peak; the rest of the diffraction pattern displays just an amorphous hump. At 800 °C the mix recrystallized with hexagonal nepheline as the main phase and minor amounts of sodalite *sensu stricto*, due to the incorporated chloride. At 1000 °C XRD indicates almost pure nepheline phase and additionally some residues of the previously introduced sodalite.

Fig. 7 shows the XRD results for MS_3.5. As for the CR_3.5 mix, virtually no changes occurred with the main phase zeolite A up to 650 °C, except a noticeable maximum of crystallinity at that temperature and the diminishment of the peak at 12.48° 2θ. At 700 °C a breakdown of the initial phases commenced, and at 750 °C almost the whole sample appeared X-ray amorphous. Compared to CR_3.5, more zeolite A residues remained as well as little amounts of sodalite. After exposure to 1000 °C XRD indicates only hexagonal nepheline.

Fig. 8 shows the XRD patterns of the sample CR_6. Almost no changes occurred up to a temperature of 650 °C. At 700 °C zeolite A started to collapse. At 750 °C a large fraction of zeolite A had been transformed into amorphous phase. Besides the remaining zeolite, like for CR_3.5 again a single reflection, matching the main peak of faujasite structures occurred in the low 2θ-range at 6.25° 2θ. After treatment at 800 °C the sample was almost completely amorphous; only three residual zeolite A peaks were observed. The unassigned peak at 6.25° 2θ disappeared. After 1000 °C the sample remained mainly amorphous, but some albite (PDF # 00-010-0393) appeared. This means that, in contrast to the previously discussed mixes, a feldspar phase with an elemental formula of $Na(Si_3AlO_8)$ was formed. This can be explained by the higher amount of silica in the CR_6 mix ($SiO_2/Al_2O_3 = 6$) compared to the other mixes.

The results for MS_6 are displayed in Fig. 9. Up to 650 °C this compositeexhibited the same behavior as the previously discussed medium- and high-silica mixes. At 700 °C the sample stayed quite crystalline, although first signs of structural breakdown were observed. No hydrosodalite was left. After treatment at 1000 °C the sample appeared X-ray amorphous.

For sample CR_3.5 additional ATR FT-IR measurements on the heat-treated samples were conducted. In particular the region between 3000 cm^{-1} and 4000 cm^{-1} (Fig. 10) is of interest for the

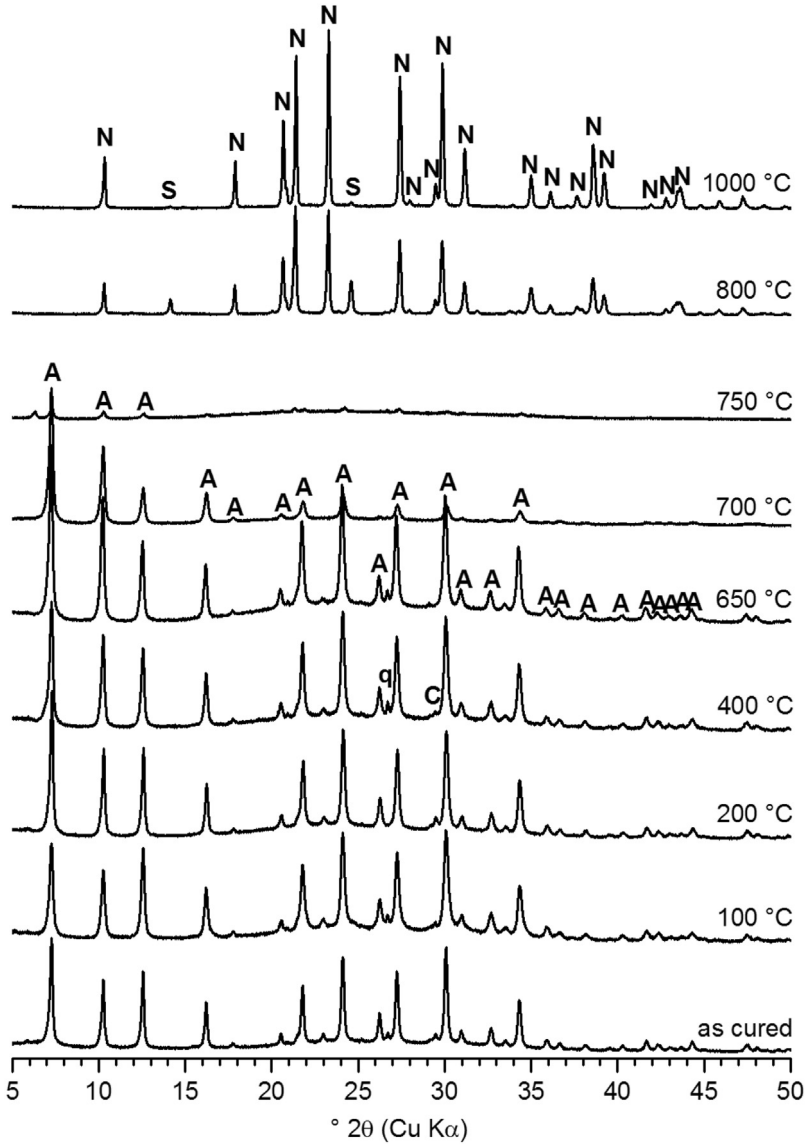

Fig. 6. Diffraction patterns of temperature-treated CR_3.5 mix. (A = zeolite A, N = nepheline, S = sodalite sensu stricto).

consideration of the dehydration, since in that range the characteristic stretching vibration centers of water and hydroxyl groups appear. At 100 °C almost no change was observed. After treatment at 150 °C, *i.e.* in the region of the most significant dehydration (Fig. 3, Table 3), the intensity reduced by almost 50%, which fits the TG results quite well. After heating to 400 °C almost the entire band disappeared, again in line with the TG results. Above 400 °C no water band remained.

Also the IR spectra below 1400 cm^{-1} (Fig. 11) fit the results of the other methods. Up to 400 °C no significant changes could be observed since the framework was stable despite dehydration. At 800 °C the IR spectrum indicated a breakdown of the original structure, as shown by the disappearance of absorption band at ~550 cm^{-1}, characteristic of zeolite A [47]. Recent investigations [48,49] have found this band in A-type zeolites to be a complex band (CB) occurring from stretching vibrations (ν_s Si-O-Si) and bending vibrations (δ O-Si-O). After heating to 1000 °C four new absorption centers (982 cm^{-1}, 702 cm^{-1}, 514 cm^{-1} and 465 cm^{-1}) occurred, which fit quite well the IR spectra of nepheline presented in Ref. [50], again in accord with the observed diffraction patterns (Fig. 6).

3.5. Compressive strength

After curing for three days at 80 °C the composites were tested for compressive strength (Fig. 12). For the MS-based samples the compressive strength correlated with the starting silica content: The higher the silica content in the starting mix (higher SiO_2/Al_2O_3 ratio), the higher was the compressive strength, in line with previous results [28]. On the contrary, the compressive strength of the CR-based composites decreased with increasing SiO_2/Al_2O_3 ratio, although this decrease was less pronounced than the increase for the MS-based samples.

Possible influences on the compressive strength of the investigated composites include the amount of non-reacted starting materials (which may act as micro-aggregates), and the relative amounts of the reaction products, *i.e.* zeolite A, hydrosodalite and geopolymeric gel in the present cases. While the amount of non-reacted silica feedstock in the composites has been determined previously [28], no quantitative data is available for the abundances of the reaction products at present. Thus, a detailed analysis of the influence of phase assemblage on the differences in compressive strength has to be conducted at a later stage. Nevertheless, it is

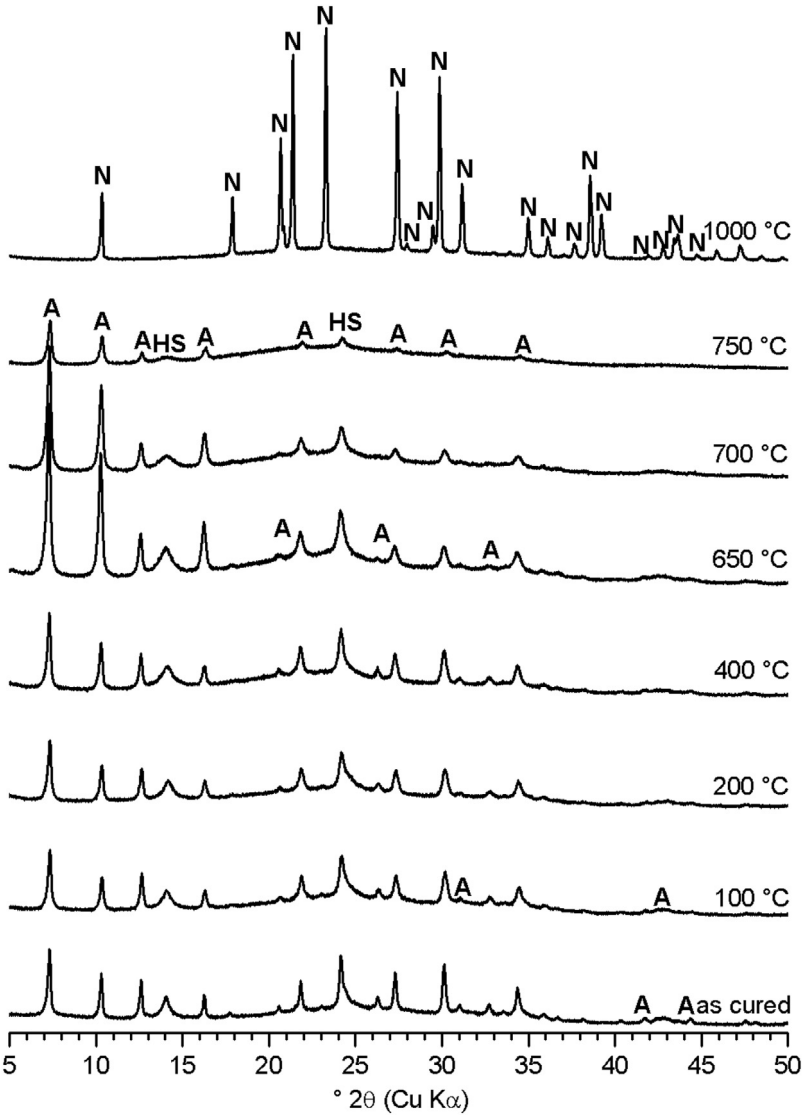

Fig. 7. Diffraction patterns of temperature-treated MS_3.5 mix. (A = zeolite A, N = nepheline, HS = hydrosodalite).

clear that the composites investigated in the present study exhibited significantly lower strength than pure geopolymers which can possess compressive strengths in excess of 80 MPa [13,51]. This is very probably related to the significant amount of crystalline zeolites in the composite materials (*cf.* Refs. [29,52]) and their porous microstructure (Section 3.7). However, the compressive strengths achieved (up to ~19 MPa) appear to be sufficient for various applications such as coatings etc.

In addition to the aforementioned influences, the (macro-)porosity of a solid is important in controlling its strength. As will be discussed below (Section 3.7), the fresh mixes exhibited swelling and macro-pore formation during curing; these processes were much more significant in the MS-based mixes, and were the more pronounced, the lower SiO_2/Al_2O_3 ratio was. This means that the macro-porosity increased with decreasing SiO_2/Al_2O_3 ratio in these materials. This behavior provides an explanation for the decrease in strength of the MS-based mixes with decreasing SiO_2/Al_2O_3 ratio. On the other hand, swelling was much less pronounced in the CR-based mixes, thus another mechanism is responsible for the dependency of strength on SiO_2/Al_2O_3 ratio. We note that at high SiO_2/Al_2O_3 ratios the workability of the CR-based pastes was considerably inferior to the workability of the MS-based pastes, and workability decreased with increasing SiO_2/Al_2O_3 ratio. This may partly explain the lower strengths of the CR-based composites at medium and high SiO_2/Al_2O_3 ratios, as insufficient workability of the fresh pastes impacts on the compressive strength of the cured composites by introducing inhomogeneities and flaws into the material.

Generally, the (residual) compressive strength of the specimens increased after thermal treatment at moderate temperatures, *i.e.* 200–400 °C, compared to the strength after curing (Figs. 13 and 14). The only exception was MS_2, which had the lowest strength after curing and no strength increase after thermal treatment as well. After treatment at temperatures ≥ 400 °C the MS_2 samples could be crumbled by hand, *i.e.* strength was virtually zero.

The strength of MS_3.5 reached a maximum after heating to 400 °C (22.7 MPa). Except for a drop at 650 °C, performance stayed almost constant up to 700 °C. At 750 °C the compressive strength decreased below the starting value. With almost 28 MPa after a treatment at 200 °C the MS_6 specimens yielded the highest strength of all samples. With further increasing temperature the compressive strength decreased. However, after heating to 400 °C it was still the mix with the highest strength, but at 650 °C the strength value decreased below the starting value, and at 750 °C

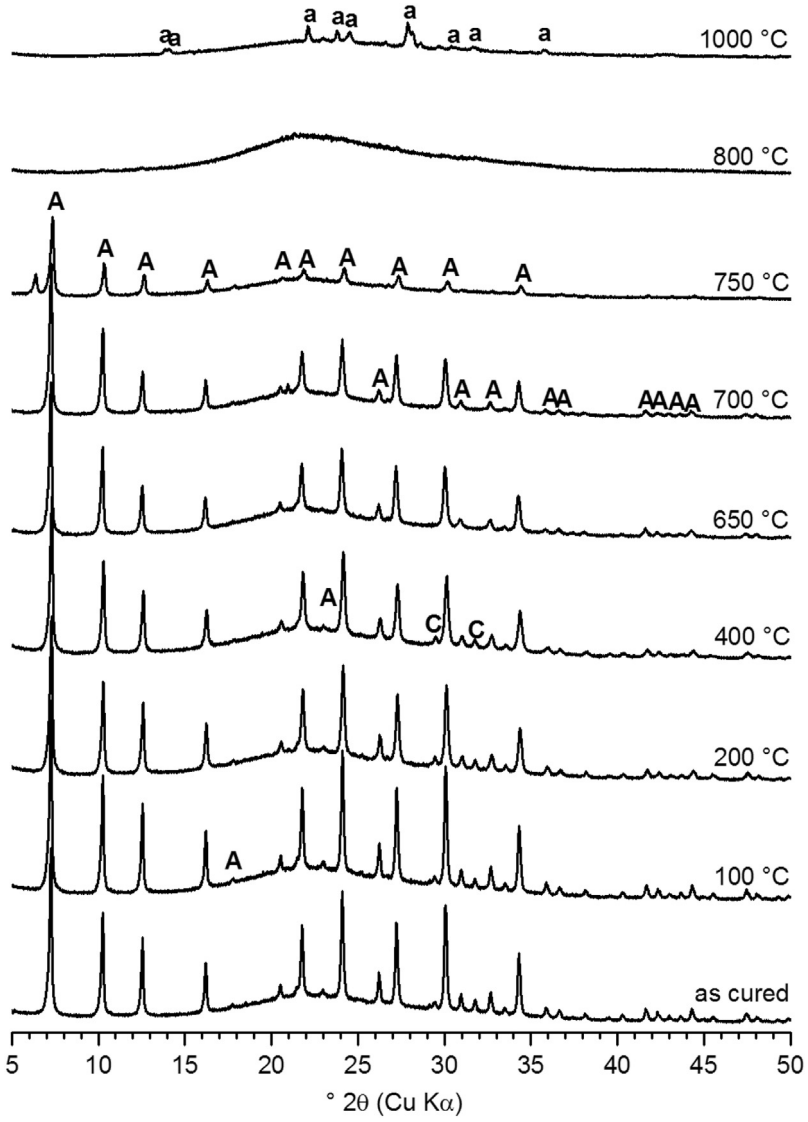

Fig. 8. Diffraction patterns of temperature-treated CR_6 mix. (A = zeolite A, a = albite, q = quartz, C = calcite).

only strength of 5 MPa remained and large deformations occurred (see Section 3.6). MS_3.5 and MS_6 mixes reached a maximum relative compressive strength of about 150% of the starting values (Fig. 14). While the performance of MS_6 continuously diminished after reaching the maximum at 200 °C, MS_3.5 retained its performance over a larger temperature range. Both mixes had residual strength of only 10 MPa (MS_3.5) and 5 MPa (MS_6) after a treatment at 750 °C.

Also the CR-based mixes increased in strength at least up to 200 °C, including the low-silica mix CR_2. These latter composites reached a maximum of 19.0 MPa after treatment at 200 °C. CR_6 reached a maximum of 15.3 MPa at 400 °C. CR_3.5 exhibited similar behavior as MS_3.5, *i.e.* strength decreased slightly at 650 °C, but increased significantly to 20.5 MPa after heating to 700 °C. This value corresponds to 195% of the strength after curing. Increasing the temperature to 750 °C resulted in massive deformations and nearly total loss of strength (Fig. 14).

Above 200 °C, the strength of CR_2 decreased successively with higher treatment temperatures down to a minimum of 8.5 MPa at 700 °C (~65% of the starting value). A further temperature increase in excess of 700 °C resulted in a regain of strength, reaching the overall maximum for this series of almost 25 MPa at 800 °C. This is equivalent to 183% of the starting strength and represents the highest compressive strength of all experiments on CR-based mixes.

CR_6 reached a relative compressive strength of 220% after heating to 400 °C. After treatment at 750 °C the strength was significantly reduced by 65% compared to the former maximum. After heating to 800 °C, a re-increase of 138% of the value measured at 750 °C was observed. At this point CR_6 reached an average strength of 20.3 MPa or 292% of the starting value. This is the highest relative increase of all considered composites caused by the thermal treatment. Remarkable is a massive, rather ductile but nevertheless crack inducing shrinkage (volume decrease) between 750 °C and 800 °C. The absolute cracking forces were the same as the ones for 750 °C but due to the smaller sample size the calculated strength increased significantly.

3.6. Dilatometry

Dilatometry experiments indicated only minor deformations in the dehydration range up to 400 °C (Fig. 15). Except MS_3.5 ($\Delta l/l \approx 2\%$) all mixes exhibited a relative linear shrinkage of $\Delta l/l \leq 1.5\%$ up to this temperature. At 650 °C a relative shrinkage of only 1.5% was observed for CR_6, while the other mixes exhibited

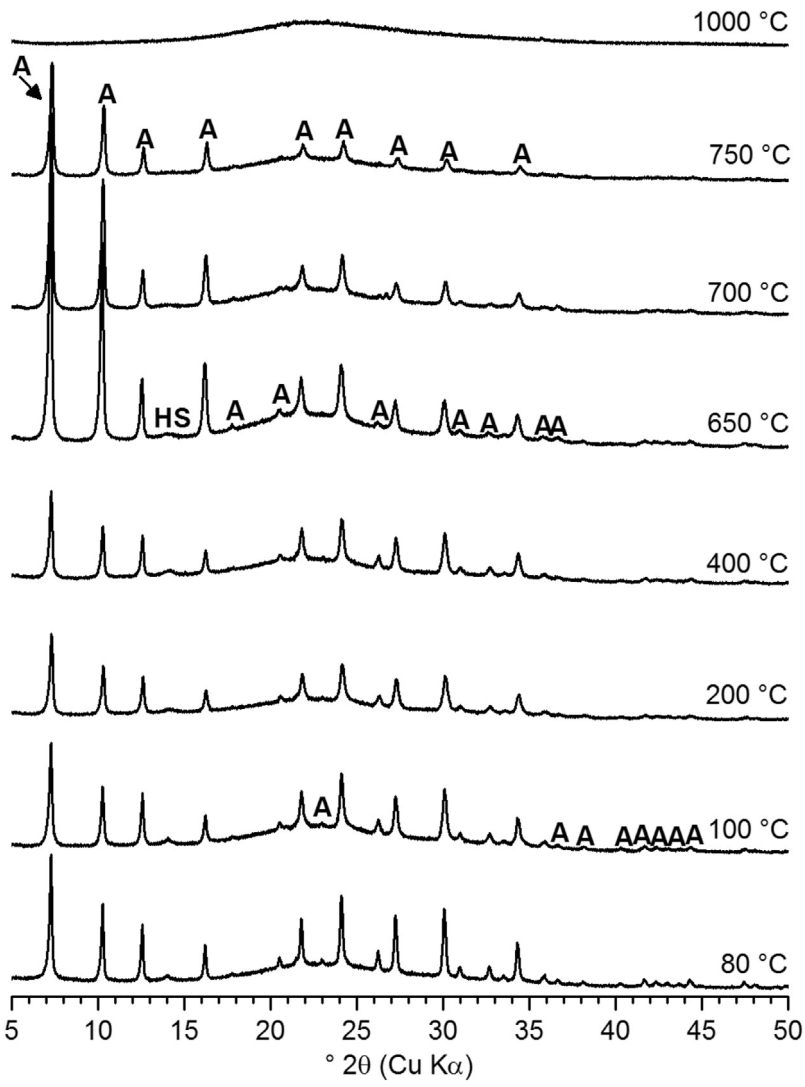

Fig. 9. Diffraction patterns of temperature-treated MS_6 mix. (A = zeolite A, HS = hydrosodalite).

somewhat higher deformations ($\Delta l/l \leq 3\%$). Up to this temperature the deformations proceeded almost linear over temperature. At ca. 700 °C the deformation-temperature curves of all samples became significantly steeper, and consequently the shrinkage increased to values of 4.2% (CR_6) to 9.5% (CR_3.5) at 800 °C. This behavior is in line with the observed deformation behavior of the cubes for the residual compressive strength tests and it correlates with the observed phase transformations above 650 °C (Section 3.4).

Above ca. 800 °C the various samples behaved quite different. The low-silica mixes yielded the lowest maximum shrinkage (CR_2 = 9.8% and MS_2 = 9.5%), while CR_3.5 reaches a maximum shrinkage of 23% at 860 °C. The CR_6 mix showed basically the same tendency but at slightly higher temperatures and with lower maximum shrinkage ($\Delta l/l$ = 16.2%). This is readily explained by the lower amount of pores in the initial state.

Medium- and high-silica MS-based mixes exhibited a differing behavior. Both had comparable shrinkage maxima ($\Delta l/l_{max}$(MS_3.5) = 17% at 840 °C and $\Delta l/l_{max}$(MS_6) = 18% at 850 °C), but with further increasing temperature the samples started to expand (MS_6: +6% and MS_3.5: +18%). In contrast to MS_2 both mixes incorporated remaining microsilica from the starting mix. This peculiar behavior of MS_3.5 and MS_6 will be discussed below (Section 4).

3.7. SEM observations

The low-silica mixes, in particular MS_2, tended to expand during curing, associated with an increased volume of air voids, *i.e.* large pores (Fig. 16, top left). Also Krivenko and Kovalchuk [53] reported that certain geopolymer mixes comprising microsilica expanded during curing, without attempting to explain this behavior. Prud'homme et al. [54] observed foam formation at 70 °C in highly alkaline aluminosiliceous systems controllable by silica fume. A hydrogen release due to the dissolution and oxidation of silicon was proposed to be the cause of this behavior. With progressing polycondensation reaction the mix became stiffer and finally initially consolidated; simultaneous ongoing hydrogen gas development resulted in foaming and swelling. This process seems to be a reason for the expansion also for the geopolymer-zeolite composites investigated in the present study. Gas release was observable as bubble formation at the surface of samples MS_2, MS_3.5, MS_6, CR_2 and CR_3.5 at the very early stage of curing at 80 °C. The expansion and the associated porosity had a considerable influence on the compressive strength, which was lowest for MS_2 and highest for MS_6, the latter being almost free of large pores (Fig. 16, top right). A possible explanation for the more pronounced expansion tendency at low SiO_2/Al_2O_3 ratios is again the higher pH of the pore solution (Section 3.1): the higher pH may

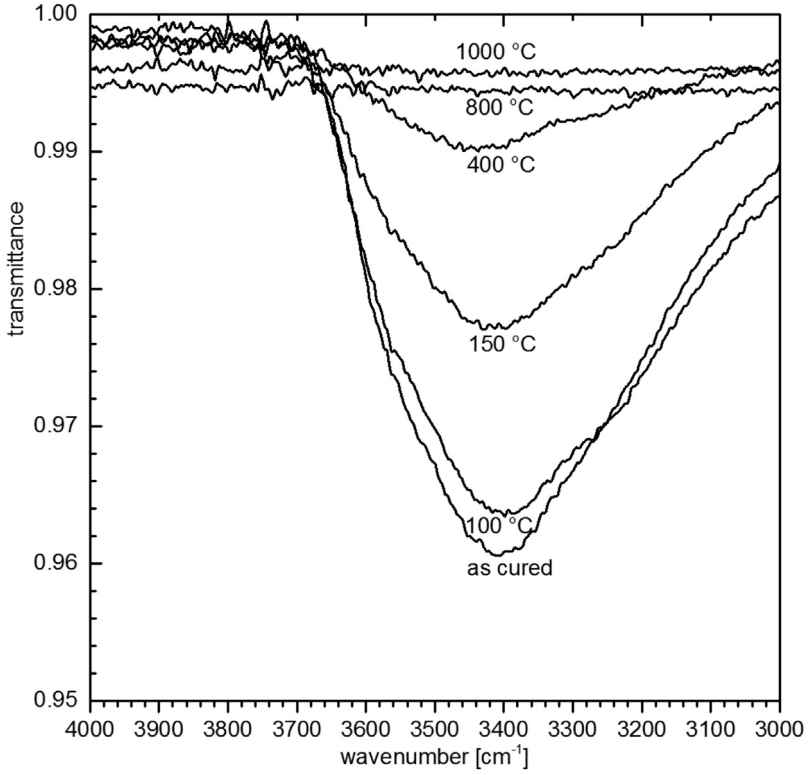

Fig. 10. ATR FT-IR spectra of selected temperature-treated CR_3.5 samples between 3000 cm^{-1} and 4000 cm^{-1}.

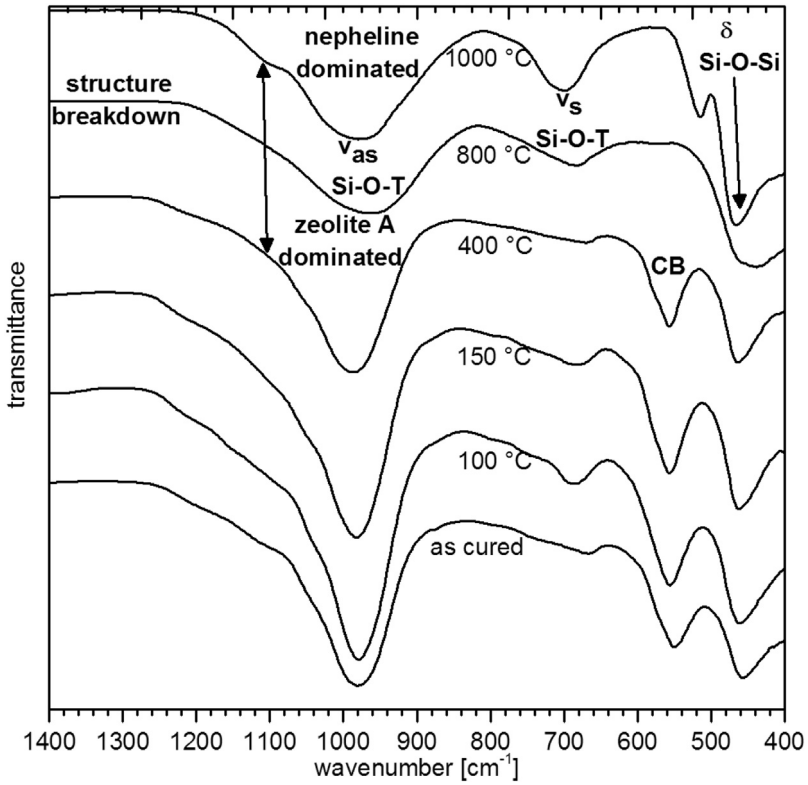

Fig. 11. ATR FT-IR spectra of selected temperature-treated CR_3.5 samples between 400 cm^{-1} and 1400 cm^{-1}. (T = Si or Al, $v_{as,s}$ = asymmetric and symmetric stretching vibration, CB = complex band; δ = bending vibration).

have caused the "foaming" reactions to proceed faster and/or to a higher extent than in the high-silica mixes, which had lower sodium aluminate fractions and consequently higher H_2O/Na_2O ratios (equal to $(H_2O/Al_2O_3)/0.98$; Table 2). Compared to the MS_2, the CR_2 samples expanded much less, which is probably a reason for their considerably higher compressive strength. The reason for

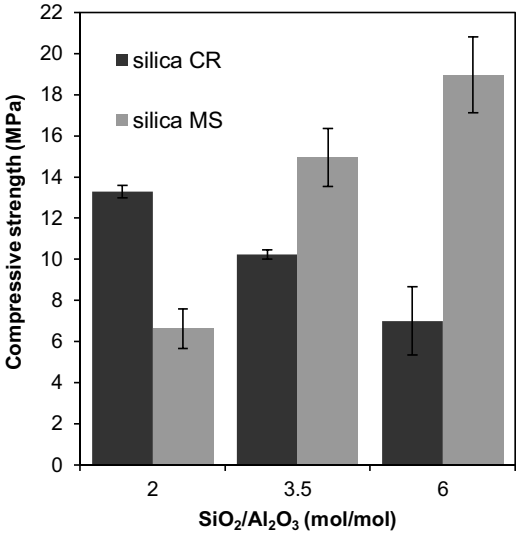

Fig. 12. Compressive strength of the composites after 3 days of curing. Error bars represent one standard deviation in each direction.

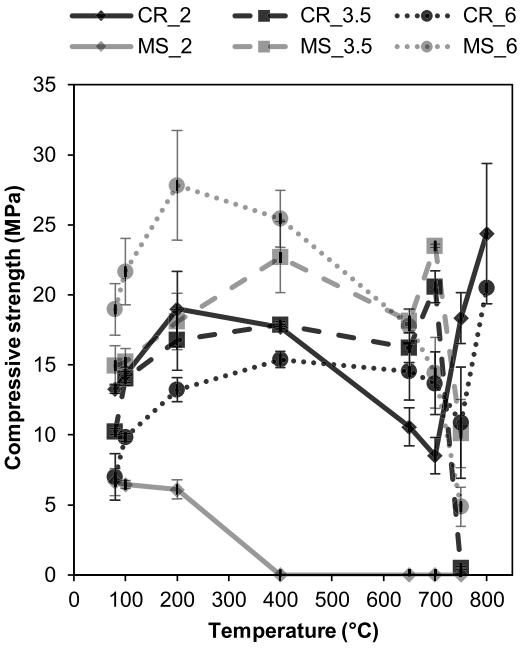

Fig. 13. Compressive strengths of the composites after 3 days of curing and thermal treatment at the specified temperatures (residual strengths). Error bars represent one standard deviation in each direction.

this difference in behavior is not clear, but it is interesting to note in this context that CR_2 contained much less hydrosodalite than MS_2. At higher magnifications, the SEM micrographs of MS_2 and MS_6 (Fig. 16, middle and bottom row) reveal a porous microstructure, consisting of particles with an approximate diameter of ca. 100 nm. This parallels previous findings on one-part geopolymer composites produced from CR-silica [26]. The microstructure of the one-part geopolymer-zeolite composites is thus much less compact than that of conventional geopolymers (*e.g.* [5,13,15,20,22,51]). As already mentioned in Section 3.5, this more porous microstructure – in connection with the high amount of crystalline zeolites in the composites – is probably responsible for the comparatively low strength of the composites under investigation, when compared to conventional geopolymers. In Fig. 16 (bottom row) it appears that

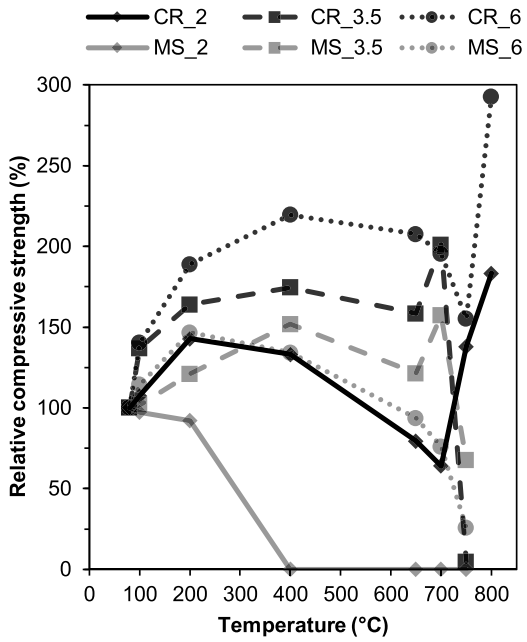

Fig. 14. Relative compressive strengths (i.e. strengths relative to the strengths after curing) of the composites after 3 days of curing and thermal treatment at the specified temperatures (residual strengths).

microstructure of MS_6 is more compact than the microstructure of MS_2, which provides an additional explanation (in addition to the lower amount of air voids) for the higher strength of MS_6.

4. General discussion of the high-temperature behavior of the composites

Thermal analysis (TG) showed that release of most of the water in the samples occurred between ca. 100 °C and 200 °C, which is the typical dehydration range of geopolymers [11,14,15,20–22,55], and some additional water loss at 200–400 °C. Comparison with the TG curve of an almost pure zeolite A (Fig. 3) and consideration of the IR spectra of the heated samples (Figs. 10, 11) as well as the deformation behavior (Fig. 15) leads to the conclusion that most of this water is of zeolitic character, in particular related to zeolite A and/or hydrosodalite. Above 400 °C only minor mass losses occurred, particularly for CR mixes, caused by escaping CO_2 from incorporated calcite. In contrast to other geopolymer systems [11,13–15,20–23,43,55], the geopolymer-zeolite composites investigated in the present study do not exhibit pronounced shrinkage in the dehydration range 100–200 °C, probably because the released water is mainly "zeolitic" water; instead, thermal shrinkage occurred rather continuously from ambient to ca. 700 °C (<3%). At temperatures above ca. 700 °C a sudden increase in shrinkage occurred. This sudden "softening" is generally attributed to viscous sintering or densification/crystallization in the geopolymers [11,13,15,20–22,55]. The rather uniform shrinkage of the specimens up to this sintering/densification temperature is considered to be an advantage in high-temperature applications. In all cases except for MS_2, thermal treatment at temperatures up to 200–400 °C caused the (residual) compressive strength of the samples to increase. Up to these temperatures no changes in phase assemblage and only subtle changes in crystallinity of the samples could be observed (Figs. 4–9). However, it has been previously established [28] that virtually no further geopolymerization occurs in the investigated mixes after one day of curing at 80 °C. Thus, the increases in strength are probably mainly related to the subtle changes in crystallinity or to other changes, not observable with

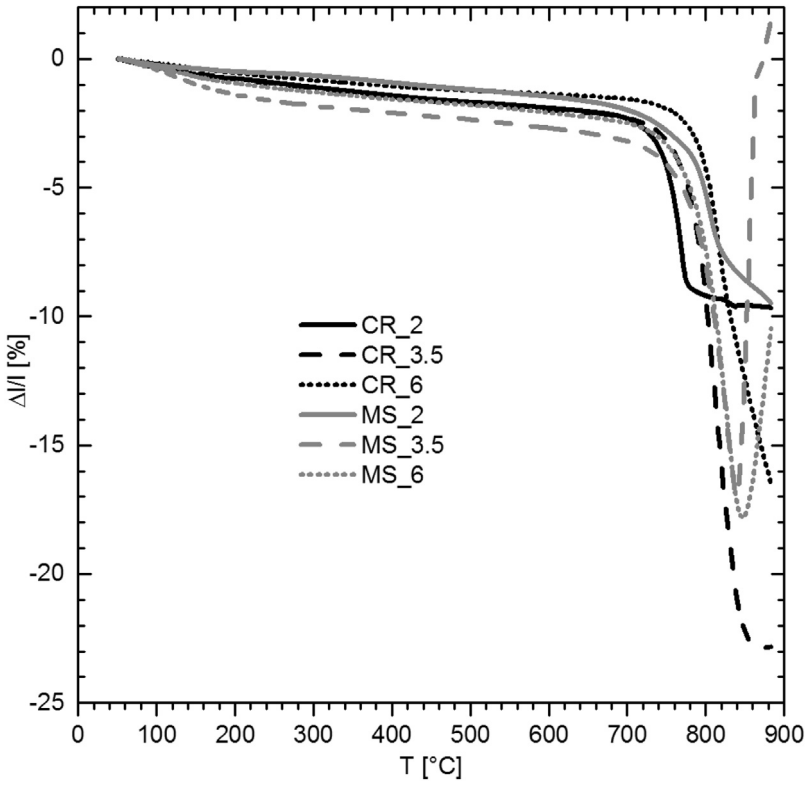

Fig. 15. Relative linear shrinkage of the cured specimens during dilatometry measurements.

XRD. The shrinkage (densification) most likely also had a positive effect on the residual strength.

Depending on the starting mix-design, phase transformations started between 400 °C and 750 °C. Except for the high-silica mixes MS_6 and CR_6, the materials transformed to stuffed silica structures of nepheline-type (MS_3.5 and CR_3.5) or a mix of nepheline and carnegieite-type silica structures (MS_2 and CR_2). This behavior parallels previous reports about aluminosiliceous precursors transforming into various stuffed silica structures [18,21,39,44,45]. MS_6 and CR_6 turned into completely amorphous or formed albite on heating to 1000 °C, respectively, the latter being a behavior that has already been reported for geopolymers with $SiO_2/Al_2O_3 = 6$ [18].

Significant changes in compressive strength could be observed after heating to temperatures that also caused significant changes in phase assemblage of the composites, particularly at temperatures of 700 °C and higher. The behavior at these temperatures varied considerably, depending on the silica feedstock and the SiO_2/Al_2O_3 ratio of the composites. MS_3.5 and CR_3.5 exhibited a strength increase on going to a treatment temperature of 700 °C and a sharp decrease afterwards (*i.e.* at 750 °C). For MS_6 only a small strength increase, followed by continuous strength deterioration was observed. On the contrary, CR_2 and CR_6 exhibited a more moderate strength loss after heating to 700 °C or 750 °C, and significant strength gain afterwards (800 °C). For CR_2 the strength gain can be mainly attributed to sintering effects, while with CR_6 the strength increase is attributed to sintering and shrinkage (the ultimate load for 800 °C was similar to the ultimate load for 750 °C, but the dimensions of the sample were smaller after 800 °C treatment). Although no strength increase was observed for MS_3.5, CR_3.5 and MS_6 in the range 700–800 °C, their residual strength evolution, *i.e.* the absence of an abrupt strength decrease up to 700 °C, is beneficial in high-temperature applications.

The peculiar behavior of MS_2, *i.e.* its decreased strength after thermal treatment at 100 °C and 200 °C and its complete loss of strength already at temperatures of 400 °C, may be related to the fact that the major crystalline phase in the specimens was hydrosodalite. Felsche and Luger [40,41] reported an increase of the volume of the unit cell of hydrosodalite during dehydration and assigned this behavior to destruction of the hydrogen bonding between hydrate water and the sodalite framework. This expansion of hydrosodalite in MS_2, restrained by shrinking zeolite A and other compounds, probably led to excessive crack formation in these samples. This assumption is supported by the dilatometry results (Fig. 15): MS_2 exhibited the lowest shrinkage of all mixes up to ca. 500 °C.

The dilatometry results showed a maximum shrinkage for medium- and high-silica MS-based mixes (MS_3.5 and MS_6) around 850 °C, followed by a sharp expansion at higher temperatures. A rapid expansion at temperatures around 600–800 °C has been observed previously for some fly ash-based geopolymers and attributed to silica gel-like products of the employed sodium silicate activating solutions [13,15,56]. In addition, Fletcher et al. [57] observed swelling of metakaolin-based geopolymers, comprising high amounts of silica (Aerosil), at temperatures of 100–300 °C. Since in the present study only samples with remaining microsilica after curing (in MS_2 the silica is virtually completely reacted [28]) showed sharp high temperature swelling, this behavior seems to be mainly caused by the residual microsilica. The CR-based samples did not exhibit extensive swelling up to the maximum measured temperature of 900 °C, which is considered to be an advantage over the MS-based mixes.

5. Conclusions

One-part geopolymer-zeolite composites were synthesized with a maximum strength of ca. 19 MPa (MS_6) after curing at 80 °C

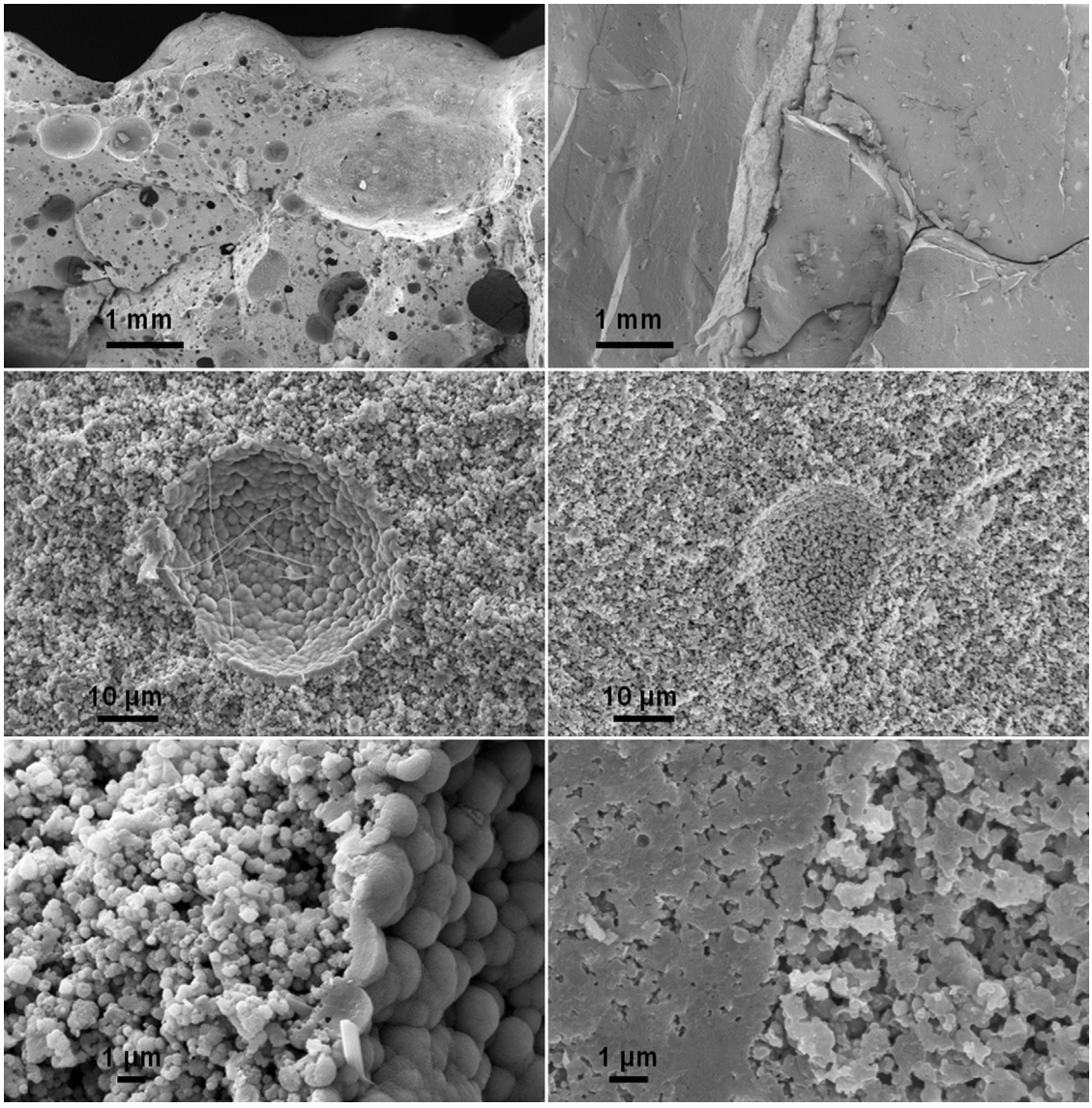

Fig. 16. SEM micrographs (secondary electrons) of fracture surfaces of the cured composites MS_2 (left column) and MS_6 (right column).

and 80% r. H. The phase content of the cured one-part mixes based on silica MS was dominated by hydrosodalite at low silica content; at high silica content zeolite A was the major crystalline phase. At the same time, swelling during curing was more significant for the low silica content. This expansion is possibly related to the formation of hydrogen during curing. The expansion reactions resulted in a high amount of large pores in the hardened specimens and correspondingly low compressive strength. The volume of large pores as well as the degree of reaction of the silica decreased with increasing silica content, with a positive effect on the compressive strength.

For the CR-based composites the crystalline phase content was always dominated by zeolite A. Differences in the phase content related to different mix-design (SiO_2/Al_2O_3 ratios) were much less significant for this feedstock. Also, differences between the mixes in expansion behavior and compressive strength were smaller; generally swelling was much less pronounced in the CR-based mixes. The CR_6 mix exhibited the lowest compressive strength, most likely related to the poor workability of this mix.

An approximately linear shrinkage was observed for the geopolymer-zeolite composites in the present investigation up to 700 °C, with the maximum shrinkage up to this temperature being ca. 2–3%. This behavior differs from the usual behavior of geopolymers, *i.e.* rapid shrinkage in the dehydration range 100–200 °C due to the release of "structural" water, making the investigated materials interesting for high-temperature applications. This observation leads to the conclusion (together with the TG results) that the incorporated water is more of zeolitic character for the investigated systems. Except for MS_2, thermal treatment at moderate temperatures (200–400 °C) led to a strength improvement up to 28 MPa (MS_6). Heating above this range led to a moderate performance loss up to 700 °C.

Above ca. 700 °C extensive shrinkage deformations occurred in all mixes. This behavior is caused by structural breakdown of the initial phase content and sintering/densification. The low-silica and medium-silica specimens underwent complex phase transformations during heating, leading to nepheline polymorphs and/or carnegieite-like phases at 1000 °C, which are of some interest for the ceramic industry. (Medium-silica mixes led to almost pure hexagonal nepheline phase.) The high-silica mixes produced an amorphous phase at 1000 °C that contained albite in addition when the silica feedstock was silica CR.

Acknowledgements

The authors thank Christian Meyer, Christiane Weimann and Patrick Klack for help with the dilatometry, SEM and ATR FT-IR measurements, respectively. P.S. acknowledges financial support from BAM within the MIS program (proposal Ideen_2012_36). The authors would also like to thank two anonymous reviewers for their insightful comments which greatly contribute to this paper and helped to improve the intelligibility of the nomenclature used.

References

[1] J. Davidovits, Geopolymers: inorganic polymeric new materials, J. Therm. Anal. 37 (1991) 1633–1656.
[2] H. Rahier, B. van Mele, M. Biesemanns, J. Wastiels, X. Wu, Low-temperature synthesized aluminosilicate glasses. Part I. Low-temperature reaction stoichiometry and structure of a model compound, J. Mater. Sci. 31 (1996) 71–79.
[3] V.F.F. Barbosa, K.J.D. MacKenzie, C. Thaumaturgo, Synthesis and characterisation of materials based on inorganic polymers of alumina and silica: sodium polysialate polymers, Int. J. Inorg. Mater. 2 (2000) 309–317.
[4] A. Palomo, S. Alonso, A. Fernandez-Jiménez, I. Sobrados, J. Sanz, Alkaline activation of fly ashes: NMR study of the reaction products, J. Am. Ceram. Soc. 87 (2004) 1141–1145.
[5] W.M. Kriven, J.L. Bell, M. Gordon, Microstructure and microchemistry of fully-reacted geopolymers and geopolymer matrix composites, Ceram. Trans. 153 (2003) 227–250.
[6] J.L. Bell, P. Sarin, P.E. Driemeyer, R.P. Haggerty, P.J. Chupas, W.M. Kriven, X-ray pair distribution function analysis of a metakaolin-based, $KAlSi_2O_6{\cdot}5.5H_2O$ inorganic polymer (geopolymer), J. Mater. Chem. 18 (2008) 5974–5981.
[7] J.L. Bell, P. Sarin, J.L. Provis, R.P. Haggerty, P.E. Driemeyer, P.J. Chupas, J.S.J. van Deventer, W.M. Kriven, Atomic structure of a cesium aluminosilicate geopolymer: a pair distribution function study, Chem. Mater. 20 (2008) 4768–4776.
[8] P. Duxson, J.L. Provis, G.C. Lukey, J.S.J. van Deventer, The role of inorganic polymer technology in the development of 'green concrete', Cem. Concr. Res. 37 (2007) 1590–1597.
[9] A. Fernandez-Jimenez, I. García-Lodeiro, A. Palomo, Durability of alkali-activated fly ash cementitious materials, J. Mater. Sci. 42 (2007) 3055–3065.
[10] C. Montes, E.N. Allouche, Evaluation of the potential of geopolymer mortar in the rehabilitation of buried infrastructure, Struct. Infrastruct. Eng. 8 (2012) 89–98.
[11] V.F.F. Barbosa, K.J.D. MacKenzie, Thermal behaviour of inorganic geopolymers and composites derived from sodium polysialate, Mater. Res. Bull. 38 (2003) 319–331.
[12] A. Fernández-Jiménez, A. Palomo, J.Y. Pastor, A. Martín, New cementitious materials based on alkali-activated fly ash: performance at high temperatures, J. Am. Ceram. Soc. 91 (2008) 3308–3314.
[13] W.D.A. Rickard, J. Temuujin, A. van Riessen, Thermal analysis of geopolymer pastes synthesised from five fly ashes of variable composition, J. Non-Cryst. Solids 358 (2012) 1830–1839.
[14] L. Vickers, W.D.A. Rickard, A. van Riessen, Strategies to control the high temperature shrinkage of fly ash based geopolymers, Thermochim. Acta 580 (2014) 20–27.
[15] W.D.A. Rickard, C.S. Kealley, A. van Riessen, Thermally induced microstructural changes in fly ash geopolymers: experimental results and proposed model, J. Am. Ceram. Soc. 98 (2015) 929–939.
[16] J. Davidovits, M. Davidovics, Geopolymer: room-temperature ceramic matrix for composites, Ceram. Eng. Sci. Proc. 9 (7/8) (1988) 835–841.
[17] D.C. Comrie, W.M. Kriven, Composite cold ceramic geopolymer in a refractory application, Ceram. Trans. 153 (2003) 211–225.
[18] P.V. Krivenko, G.Y. Kovalchuk, Directed synthesis of alkaline aluminosilicate minerals in a geocement matrix, J. Mater. Sci. 42 (2007) 2944–2952.
[19] P.V. Krivenko, Y.K. Pushkavera, M.V. Sukhanevich, S.G. Guziy, Fireproof coatings on the basis of alkaline aluminum silicate systems, Ceram. Eng. Sci. Proc. 29 (10) (2009) 129–142.
[20] J.L. Bell, P.E. Driemeyer, W.M. Kriven, Formation of ceramics from metakaolin-based geopolymers: part I—Cs-based geopolymer, J. Am. Ceram. Soc. 92 (2009) 1–8.
[21] C. Kuenzel, L.M. Grover, L. Vandeperre, A.R. Boccaccini, C.R. Cheeseman, Production of nepheline/quartz ceramics from geopolymer mortars, J. Eur. Ceram. Soc. 33 (2013) 251–258.
[22] J.L. Bell, P.E. Driemeyer, W.M. Kriven, Formation of ceramics from metakaolin-based geopolymers. Part II: K-based geopolymer, J. Am. Ceram. Soc. 92 (2009) 607–615.
[23] C. Kuenzel, L.J. Vandeperre, S. Donatello, A.R. Boccaccini, C. Cheeseman, Ambient temperature drying shrinkage and cracking in metakaolin-based geopolymers, J. Am. Ceram. Soc. 95 (2012) 3270–3277.
[24] A. Hajimohammadi, J.L. Provis, J.S.J. van Deventer, One-part geopolymer mixes from geothermal silica and sodium aluminate, Ind. Eng. Chem. Res. 47 (2008) 9396–9405.
[25] A. Hajimohammadi, J.L. Provis, J.S.J. van Deventer, Effect of alumina release rate on the mechanism of geopolymer gel formation, Chem. Mater. 22 (2010) 5199–5208.
[26] G.J.G. Gluth, C. Lehmann, K. Rübner, H.-C. Kühne, Geopolymerization of a silica residue from waste treatment of chlorosilane production, Mater. Struct. 46 (2013) 1291–1298.
[27] X. Ke, S.A. Bernal, N. Ye, J.L. Provis, J. Yang, One-part geopolymers based on thermally treated red mud/NaOH blends, J. Am. Ceram. Soc. 98 (2015) 5–11.
[28] P. Sturm, S. Greiser, G.J.G. Gluth, C. Jäger, H.J.H. Brouwers, Degree of reaction and phase content of silica-based one-part geopolymers investigated using chemical and NMR spectroscopic methods, J. Mater. Sci. 50 (2015) 6768–6778.
[29] D. Koloušek, J. Brus, M. Urbanova, J. Andertova, V. Hulinsky, J. Vorel, Preparation, structure and hydrothermal stability of alternative (sodium silicate-free) geopolymers, J. Mater. Sci. 42 (2007) 9267–9275.
[30] P. Duxson, J.L. Provis, Designing precursors for geopolymer cements, J. Am. Ceram. Soc. 91 (2008) 3864–3869.
[31] E. Königsberger, P.M. May, G. Hefter, Comprehensive model of synthetic *Bayer* liquors. Part 3. Sodium aluminate solutions and the solubility of gibbsite and boehmite, Monatsh. Chem. 137 (2006) 1139–1149.
[32] J.L. Provis, G.C. Lukey, J.S.J. van Deventer, Do geopolymers actually contain nanocrystalline zeolites? A reexamination of existing results, Chem. Mater. 17 (2005) 3075–3085.
[33] B. Zhang, K.J.D. MacKenzie, I.W.M. Brown, Crystalline phase formation in metakaolinite geopolymers activated with NaOH and sodium silicate, J. Mater. Sci. 44 (2009) 4668–4676.
[34] D.W. Breck, Zeolite Molecular Sieves, Wiley, New York, 1974.
[35] C.S. Cundy, P.A. Cox, The hydrothermal synthesis of zeolites: precursors, intermediates and reaction mechanism, Microporous Mesoporous Mater. 82 (2005) 1–78.
[36] J. Weitkamp, R. Schumacher, U. Weiß, Hydrothermalsynthese und Charakterisierung von Zeolith EMT, Chem. Ing. Tech. 64 (1992) 1109–1112.
[37] M.M.J. Treacy, J.B. Higgins, Collection of Simulated XRD Powder Patterns for Zeolites, 4th revised edn., Elsevier, Amsterdam, 2001.
[38] B. Subotić, D. Škrtić, I. Šmit, L. Sekanović, Transformation of zeolite A into hydroxysodalite: I. An approach to the mechanism of transformation and its experimental evaluation, J. Cryst. Growth 50 (1980) 498–508.
[39] A. Radulović, V. Dondur, P. Vulić, Z. Miladinović, G. Ćirić-Marjanović, R. Dimitrijević, Routes of synthesis of nepheline-type polymorphs: an influence of Na-LTA bulk composition on its thermal transformations, J. Phys. Chem. Solids 74 (2013) 1212–1220.
[40] J. Felsche, S. Luger, Phases and thermal decomposition characterisitics of hydro-sodalites $Na_{6+x}[AlSiO_4]_6(OH)_x{\cdot}nH_2O$, Thermochim. Acta 118 (1987) 35–55.
[41] J. Felsche, S. Luger, Structural collapse or expansion of the hydro-sodalites series $Na_8[AlSiO_4]_6(OH)_2{\cdot}nH_2O$ and $Na_6[AlSiO_4]_6{\cdot}nH_2O$ upon dehydration, Ber. Bunsenges. Phys. Chem. 90 (1986) 731–736.
[42] G. Engelhardt, J. Felsche, P. Sieger, The hydrosodalite system $Na_{6+x}[SiAlO_4]_6(OH)_x{\cdot}nH_2O$: formation, phase composition, and de- and rehydration studied by ^{1}H, ^{23}Na, and ^{29}Si MAS–NMR spectroscopy in tandem with thermal analysis, X-ray diffraction, and IR spectroscopy, J. Am. Chem. Soc. 114 (1992) 1173–1182.
[43] A. Buchwald, M. Vicent, R. Kriegel, C. Kaps, M. Monzó, A. Barba, Geopolymeric binders with different fine fillers—phase transformations at high temperatures, Appl. Clay Sci. 46 (2009) 190–195.
[44] J.G. Thompson, A. Melnitchenko, S.R. Palethorpe, R.L. Withers, An XRD and electron diffraction study of cristobalite-related phases in the $NaAlO_2$–$NaAlSiO_4$ system, J. Solid State Chem. 131 (1997) 24–37.
[45] J.G. Thompson, R.L. Withers, A. Melnitchenko, S.R. Palethorpe, Cristobalite-related phases in the $NaAlO_2$–$NaAlSiO_4$ system. I. Two tetragonal and two orthorhombic structures, Acta Crystallogr. B 54 (1998) 531–546.
[46] M. Okrusch, S. Matthes, Mineralogie: Eine Einführung in die spezielle Mineralogie, in: Petrologie und Lagerstättenkunde, 9th edn., Springer, Berlin, 2014.
[47] E.M. Flanigen, H. Khatami, H.A. Szymanski, Infrared structural studies of zeolite frameworks, in: E.M. Flanigen, L.B. Sand (Eds.), Molecular sieve zeolites–I, Adv. Chem. Ser. 101, American Chemical Society Washington, D.C., (1971) 201–229.
[48] W. Mozgawa, W. Jastrzebski, M. Handke, Vibrational spectra of D4R and D6R structural units, J. Mol. Struct. 744–747 (2005) 663–670.
[49] W. Mozgawa, M. Król, K. Barczyk, FT-IR studies of zeolites from different structural groups, Chemik 65 (2011) 671–674.
[50] H.H.W. Moenke, Silica, the three-dimensional silicates, borosilicates and beryllium silicates, in: V.C. Farmer (Ed.), The Infrared Spectra of Minerals, Mineralogical Society, London, 1974, pp. 365–382.
[51] P. Duxson, J.L. Provis, G.C. Lukey, S.W. Mallicoat, W.M. Kriven, J.S.J. van Deventer, Understanding the relationship between geopolymer composition, microstructure and mechanical properties, Colloids Surf. A 269 (2005) 47–58.
[52] S.J. O', Connor, K.J.D. MacKenzie, Synthesis, characterisation and thermal behavior of lithium aluminosilicate inorganic polymers, J. Mater. Sci. 45 (2010) 3707–3713.
[53] P.V. Krivenko, G.Y. Kovalchuk, Fly-ash based zeolite cements, in: R.K. Dhir, P.C. Hewlett, L.J. Csetenyi (Eds.), Innovations and Developments in Concrete Materials and Construction, Thomas Telford, London, 2002, pp. 123–132.
[54] E. Prud'homme, P. Michaud, E. Joussein, C. Peyratout, A. Smith, S. Arrii-Clacens, J.M. Clacens, S. Rossignol, Silica fume as porogent agent in geo-materials at low temperature, J. Eur. Ceram. Soc. 30 (2010) 1641–1648.

[55] P. Duxson, G.C. Lukey, J.S.J. van Deventer, Physical evolution of Na-geopolymer derived from metakaolin up to 1000 °C, J. Mater. Sci. 42 (2007) 3044–3054.
[56] J.L. Provis, C.Z. Yong, P. Duxson, J.S.J. van Deventer, Correlating mechanical and thermal properties of sodium silicate-fly ash geopolymers, Colloids Surf. A 336 (2009) 57–63.
[57] R.A. Fletcher, K.J.D. MacKenzie, C.L. Nicholson, S. Shimada, The composition range of aluminosilicate geopolymers, J. Eur. Ceram. Soc. 25 (2005) 1471–1477.